Data-driven method to assess the influence of process parameters on the fatigue response of additively manufactured Ti6Al4V

Available online at www.sciencedirect.com

ScienceDirect

Procedia Structural Integrity 47 (2023) 56–69

Structural Integrity Procedia

www.elsevier.com/locate/procedia

27th International Conference on Fracture and Structural Integrity (IGF27)

Data-driven method to assess the influence of process parameters on the fatigue response of additively manufactured Ti6Al4V

Alberto Ciampaglia[a,*], Andrea Tridello[a], Filippo Berto[b], Davide Paolino[a]

[a]*Department of Mechanical and Aerospace Engineering, Politecnico di Torino, C.so Duca degli Abruzzi 24, 101219, Torino, Italy*
[b]*Department of Chemical Engineering Materials Environment, Sapienza University of Rome, Via Eudossiana 18, 00184, Roma, Italy*

Abstract

The fatigue behavior of Additive Manufacturing (AM) parts is influenced by manufacturing defects, whose dimensions are primarily determined by the parameters of the AM process, which, in turn, also affect the resulting microstructure, together with heat treatments. This study employs Machine Learning (ML) techniques to forecast the fatigue response of AM parts from the AM process variables and the heat treatment characteristics. Feed-forward neural networks (FFNN) and physics-informed neural network (PINN) models are formulated and verified employing published datasets on AM Ti6Al4V alloy. The results demonstrate that physics-based ML approaches are effective in forecasting the fatigue response of AM components.

Keywords: Type your keywords here, separated by semicolons ;

1. Introduction

The design of metal components to be produced with Additive manufacturing (AM) technology gives space to innovative structural solutions, reducing the waste of material and allowing for the tuning of the material properties with the use, for example, of lattice structures. However, AM parts produced with Selective Laser Melting (SLM) process are characterized by numerous and large defects originating from the manufacturing, like pores, lack of fusion,

* Corresponding author.
E-mail address: alberto.ciampaglia@polito.it

10.1016/j.prostr.2023.06.041

trapped gas (Tridello et al., 2021). Under cyclic loadings, these microstructural irregularities act as nucleation sites where the fatigue crack starts propagating and eventually leads to a catastrophic failure of the component(Molaei & Fatemi, 2018; Murakami et al., 2019; Yadollahi & Shamsaei, 2017; Yamashita et al., 2018). The quality of AM parts has significantly improved in last years, with a substantial reduction of the defectiveness, but the formation of manufacturing induced defects is unavoidable due to the nature of the additive technology.

The design of parts undergoing fatigue loads requires therefore a damage tolerant approach, meaning that the intrinsic material defectiveness must be accounted for, and appropriate models need to be developed to assess the influence of the defects on the fatigue response. The most common damage-tolerant methodologies in the field of fatigue design originate from the Murakami's theory, which correlates the fatigue strength with the defect size and the material hardness through a semi-empirical relation(du Plessis & Beretta, 2020; Meneghetti et al., 2019; Romano et al., 2019). To assess the fatigue strength using these models, a characterization of the size and the shape of the critical defects inside the component is needed beforehand, e.g., with micro-CT scans of the manufactured parts or with destructive metallographic inspections. For AM parts, in which the defect properties are mainly influenced by the processing parameters, the characterization of the internal defectiveness should be carried out for any set of parameter configurations, but this would be not feasible due to cost and time constraints. The effect of the AM processing parameters on the internal defects is complex and has been experimentally investigated by numerous research, which revealed that the main parameters governing the defectiveness of the parts are the beam diameter, beam power, layer thickness, powder size, scanning speed, building angle, hatch distance, and power. Modelling the effect of these parameters, and their interactions, on the formation of porosities or microstructural imperfections would require a multiparameter model that should be calibrated through an extensive design of experiments, whose realization would result unfeasible.

The problem of discovering a relationship between numerous and interacting parameters on the fatigue response opens the door to the adoption of Machine Learning (ML) algorithms that can leverage the availability of several experimental findings on the effect of the single parameters on the response of Ti6Al4V parts produced with AM in the literature. In the last years, ML models have been developed to surrogate numerical models for the prediction of the fatigue response of SS216L and Ti6Al4V produced with SLM (J. Li et al., 2022; Zhan & Li, 2021a, 2021b), to model the effect of shot-peening and thermal treatments for AlSi10Mg (Maleki et al., 2022), and to give a probabilistic prediction of the fatigue response of Ti6Al4V from the manufacturing parameters(Chen & Liu, 2021).

In this paper, ML algorithms have been designed to combine the predictive capability of the neural networks (NN) with the empirical knowledge described by Murakami's theory, to assess the fatigue response of the Ti6Al4V parts: a database containing information found in the literature on the manufacturing process parameters, the stress amplitude, and the number of cycles at failure has been used to train a physics-informed neural network (PINN) whose architecture mimics the Murakami's formulation.

In Section 2, a description of the data collected in the literature is given and the main findings reported in the relative works are summarised. In section 3 a basic NN and a PINN model developed by (Ciampaglia et al., 2023) are introduced, whose results are discussed in Section 3.

Nomenclature

ML	Machine learning
NN	Neural network
PINN	Physics-informed neural network
AM	Additive manufacturing
SLM	Selective Laser Melting

2. Materials

The methodology described in this paper is used to predict the fatigue response of the Ti6Al4V alloy produced with SLM process. To assess the relationship between the manufacturing parameters and the fatigue strength S at N_f cycles, a database containing data available in the literature has been built.
The dataset used to train the ML models is composed of 768 data points (Table 1), each defined as a set of process parameters, heat treatment parameters, stress amplitude and the number of cycles at failure. The stress amplitude at stress ratio $R = -1$ is considered in the following analysis. If the experimental literature data have been obtained through tests at different stress ratios, the "Smith-Watson-Topper" (SWT) correction has been applied to assess the equivalent stress amplitude $s_{a,eq}$ at R=-1 (i.e., $s_{a,eq} = s_{max} \cdot \sqrt{\frac{1-R}{2}}$, being s_{max} the maximum applied stress in a load cycle).

Table 1. The main process parameters of the literature data collected in the database:

Ref.	Orientation [°]	Power [W]	Hatch [mm]	Speed [mm/s]	Layer thickness [µm]
(Du et al., 2021)	90	120	0.07	1200	30
	90	120	0.1	1000	45
	90	120	0.13	800	60
	90	160	0.13	1000	30
	90	160	0.07	800	45
	90	160	0.1	1200	60
	90	200	0.1	800	30
	90	200	0.13	1200	45
	90	200	0.07	1000	60
	90	160	0.07	1000	30
(Günther et al., 2017)	90	175	0.12	710	30
(Hu et al., 2020)	90	280	0.14	1200	30
(P. Li et al., 2016)	0	200	0.18	200	50
	90	375	0.12	1029	60
	0	375	0.12	1029	60
	90	375	0.12	1029	60
	0	175	0.125	710	30
	90	250	0.06	1600	30
	90	200	0.25	1250	40
(Sanaei & Fatemi, 2020)	90	400	0.16	1000	50
	90	285	0.14	1200	30
	45	285	0.14	1200	30
(Zhao et al., 2016)	90	200	0.1	1000	50

(Fousová et al., 2018)	90	200	0.08	1250	30
(Jiang et al., 2021)	0	190	0.065	1000	30
(Sun et al., 2021)	90	360	0.1	1200	60
(Günther et al., 2018)	90	175	0.12	710	30
(Eric et al., 2013)	45	170	0.1	1250	30
(Gong et al., 2015)	90	120	0.1	960	30
	90	120	0.1	540	30
	90	120	0.1	400	30
	90	120	0.1	1260	30
	90	120	0.1	1500	30
(Alegre et al., 2022)	90	400	0.12	150	60
(Macallister & Becker, 2022)	90	170	0.1	1200	30
(Mertova et al., 2018)	90	200	0.08	1250	30
(Moran et al., 2022)	45	160	0.14	1200	30
	45	245	0.082	1250	60
	45	280	0.14	1200	30
	45	245	0.082	1250	60
(Soltani-Tehrani et al., 2022)	90	280	0.14	1200	30
(Yan et al., 2019)	90	280	0.05	1200	30
(Kumar & Ramamurty, 2020)	90	280	0.14	1200	30
	90	340	0.12	1250	60

The manufacturing parameters collected in the analyzed database are the orientation, the input power, the hatch distance, the speed, and the layer thickness. Two thermal treatments are moreover generally adopted in the literature:

- Annealing: conducted at a temperature between 600°C and 800° with a duration that spans from half to two hours, this treatment can relieve the residual stress induced by the repeated welding and refine the microstructure.
- Hot Isostatic Pressing (HIP): thermo-mechanical treatment where a pressure of 1000 bar is applied at temperatures above 900°C for two hours or more. The HIP process allows to reduce the porosity of the parts, yielding an enhancement of the fatigue performance.

The main surface treatments applied to the Ti6Al4V are sandblasting (SB), shot peening (SP), laser shot peening (LSP), surface mechanical attrition treatment (SMAT), electric discharge machining (EDM) and surface polishing. A column for each treatment has been added to the database, with a boolean value indicating if the data has been subjected to a specific treatment or not.

3. Method

The fatigue response of materials is commonly described by a relation between the applied load, referred as the stress amplitude S, and the number of cycles at failure, referred to as N_f. The proposed model expands the standard relations by introducing the correlation between the manufacturing parameters and the fatigue response, which is implicitly controlled by the internal defectiveness. To define this relation, two ML models are designed: a NN with standard architecture, and a PINN with an architecture inspired to the Murakami theory.

3.1. Neural Network (NN)

Probably, the most common supervised ML method, NN are trainable numerical models with a layered architecture, where the information is propagated from the input to the output layer through a network of neurons. Every neuron is fully connected to the previous layers and performs the elementary operation on the inputs x_i:

$$y = \mathcal{A}(\sum w_i x_i + b)\,, \tag{1}$$

where x_i is the input of the i-th connection, b is the bias of the neuron, and $\mathcal{A}(\cdot)$ is the activation function. The weight and bias of the network are the trainable parameters, while the number of neurons of each layer, the number of layers and the activation functions are the hyperparameters that need to be a-priori defined. The most common activation functions are the Rectified Linear Unit (ReLU), the hyperbolic tangent, and the sigmoid function; these functions allow for the activation of the neuron, replicating the firing mechanism of the brain's neurons, and introduce a non-linearity in the model that would otherwise be equivalent to a linear regression.

Being a supervised method, the NN is trained on a set of data whose input and output are both known. The training process starts with a random initialization of the parameters, thereafter the information is propagated from the input to the output, where a loss function computes the error. The error is then backpropagated to the neurons, where a gradient descent algorithm is used to update the values of the parameters based on the distributed error. The forward prediction and back propagation are iteratively repeated on a subset of the data (i.e., a batch) until a convergence criterion is reached. The predictive capability of this Neural Network architecture is compared with the predictive capability of the Physics-informed Neural Network (PINN) described in the following Section.

3.2. Physics-informed Neural Network (PINN)

The PINN developed in this paper is inspired by the Murakami's fomulation, which models the relationship between the fatigue strength S, the square root of the area of the defect, $\sqrt{a_c}$, projected in a direction perpendicular to the maximum tensile stress, and the Vicker's hardness HV :

$$S = \frac{C_1(HV + 120)}{\left(\sqrt{a_c}\right)^{\frac{1}{6}}}\,, \tag{2}$$

where C_1 is a coefficient accounting for the influence of the defect location (i.e., surface defects are more critical than internal defects since characterized by a larger stress intensity factor). Eq. 2 correlates the defect size, which negatively affects the fatigue strength, and the hardness, dependent on the material microstructural properties. Although this relationship has been developed for traditionally built materials, in particular high-strength steels with spherical inclusions, (Masuo et al., 2018) demonstrated its applicability to AM parts provided that an equivalent defect size in place of the actual one is considered. Eq. 2 has been moreover rearranged in the literature to model the dependency between the fatigue life and the defect size (Mayer et al., 2014; Murakami, 2019; Paolino et al., 2016). A general expression modelling the relationship between the fatigue life and the defect size, according to the Basquin's law and the Murakami's formulation, is reported in Eq. 3:

$$S = \frac{C_1(HV + 120)}{\sqrt{a_c}^{\frac{1}{6}}} C_2 N_f^k \,, \tag{3}$$

where the C_2 and k are empirical parameters to be experimentally fitted.
As for the other metallic materials produced through AM process, the defectiveness of Ti6Al4V parts is mainly governed by the manufacturing process, whereas the material microstructure is controlled both by the AM process parameters and by the subsequent thermal treatments (Tridello & Paolino, 2020). Accordingly, the process parameters and the heat treatment properties should be considered as input when modelling the fatigue response of AM parts, according to Eq. 3, and, in particular, of the investigated Ti6Al4V alloy.
The proposed PINN mimics the chain of causality describing the process-structure-property relation that governs the fatigue response of AM parts, by adopting an architecture introduced in (Ciampaglia et al., 2023) made of two branches that estimate the effect of the process parameters on the defectiveness and the microstructure, respectively. The two main PINN sub-network are described below:

- MicroNet: vector of variables ϕ (build orientation, hatch distance, speed, energy density, power input, layer thickness, beam diameter and plate temperature, duration and temperature of the thermal treatment, surface treatment) feeds the neural network $\mathbb{N}^1$ that predicts the microstructural strength parameter.
- DefectNet: vector of variables θ (build orientation, hatch distance, speed, energy, power, layer thickness, beam diameter and plate temperature) feeds the neural network $\mathbb{N}^2$ predicting the effect of these parameters on the defect size.

According to Eq. 3, the fatigue strength, defined as the stress value at which the failure occurs after N_f cycles, is proportional to the microstructural strength and inversely proportional to the defect area. Based on this empirical knowledge, the ratio of the DefectNet output over the MicroNet output is computed inside a custom layer of the PINN and propagated to a trainable layer, as shown in Figure 1.

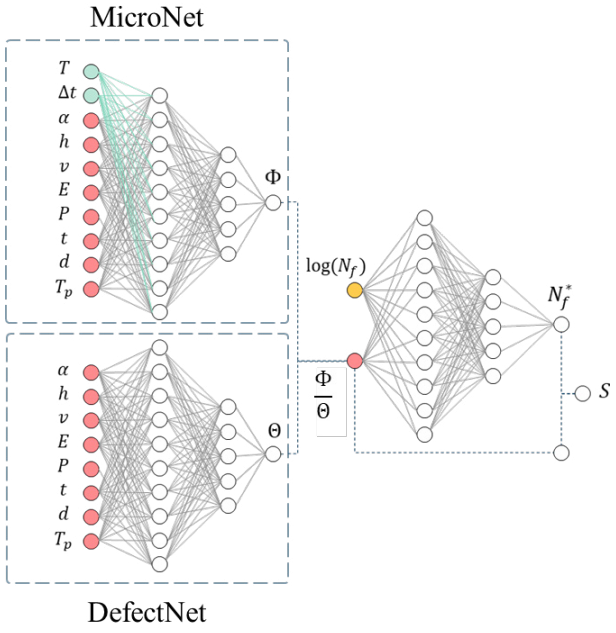

Figure 1. Schematic representation of the modular PINN.

The final layers learn a correlation between the latent variables computed with the sub-nets, the number of cycles and

the fatigue strength:

$$S = \frac{\mathbb{N}^1(\phi; w_\theta, b_\theta)}{\mathbb{N}^2(\theta; w_\phi, b_\phi)} \left(\frac{w_C^1}{N_f}\right)^{w_C^2} = \frac{\Theta}{\Phi} \left(\frac{w_C^1}{N_f}\right)^{w_C^2} \tag{4}$$

The PINN is trained to minimize the loss function described with Eq. 5:

$$\mathcal{L} = \frac{1}{N} \left| S - \frac{\mathbb{N}^1(\phi; w_\theta, b_\theta)}{\mathbb{N}^2(\theta; w_\phi, b_\phi)} \left(\frac{w_C^1}{N_f}\right)^{w_C^2} \right|_{F2}, \tag{5}$$

where the operator $|\cdot|_{F2}$ is the Frobenius norm. The trainable parameters w_{ci} are deputed to model the shape of the fatigue curve depending on the process parameters.

The designed PINN intrinsically complies with the S-N monotonicity constraint, being the derivative of the output layer with respect to the number of cycles always negative.

4. Results and discussion

4.1. NN results

The structure of the NNs developed without embedding any physical knowledge (Section 2.1) is summarised in **Error! Reference source not found.**.

Table 2. Summary of FFNN optimized structures with activation function and number of neurons of each layer

Layer	Neurons	Activation function	Output shape
Input	6	ReLU	(6, 1)
Dense 1	50	ReLU	(50, 1)
Dense 2	50	ReLU	(50, 1)
Dense 3	40	ReLU	(40, 1)
Output	40	ReLU	(1, 1)

The input layer is connected to the model inputs, namely building orientation, energy, beam diameter, hatch distance, layer thickness, number of cycles, and plate temperature. The NN is trained with 80% of the available data, while the remaining 20% is used as validation to check that the network is not overfitting the training observations. The loss function has been defined as the Mean Square Error (MSE) of the fatigue strength, which has been minimized with the adaptive optimizer algorithm Adam with a learning rate of 0.07 and an exponential decay rate of 0.9. The training has been iterated until a decrease lower than the 2% is observed for 20 consecutive iterations.

The value of the loss function for the training and validation data during the training process is shown in Figure2a, whereas Figure 2b shows an accuracy plot which compares the fatigue strength predicted with the NN (S_{NN}) with the experimental values (S_{exp}). In Figure 2b, an error band of ±150 MPa and a Normal distribution with standard deviation of 50MPa are also shown.

a) b)

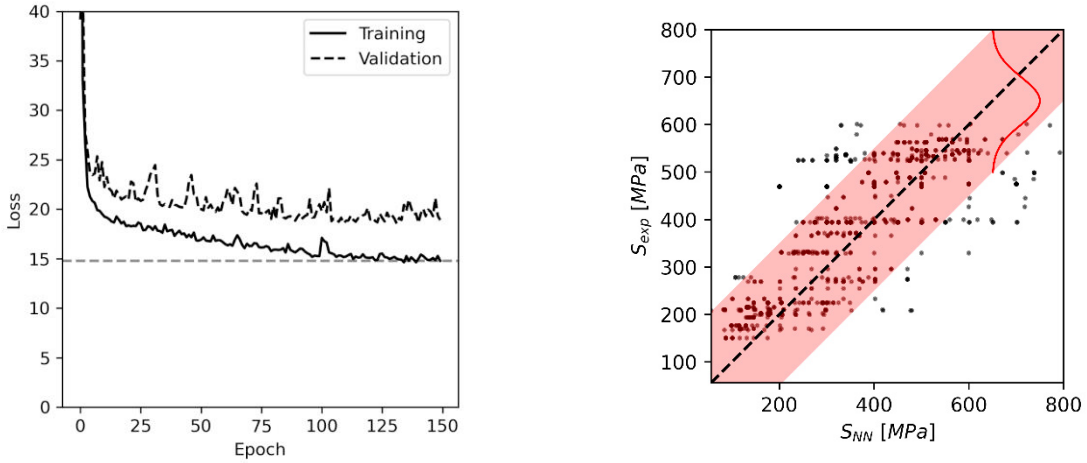

Figure 2. a) Training and validation loss during the training of the NN; b) accuracy plot comparing the stress predicted with the NN (S_{NN}) with the experimental one (S_{exp}).

The NN correlates the process parameters to the fatigue performance with a 70 % average error and a 270% maximum error. According to Figure 2b, the majority of the data are within the error band, but many data are also far from the bisector and outside this range, due to the stochastic nature of the fatigue behaviour, especially when driven by defects.

4.2. PINN results

The PINN model is composed of two main branches: the DefectNet and the MicroNet, which predict the effect of the process variables on the material defectiveness and the resultant microstructure, respectively. Both sub-networks have 2 hidden layers, with 10 and 5 neurons, respectively; the output network that computes the fatigue strength from the number of cycles and the latent variables in output from the two branches, has again 2 hidden layers with 10 and 5 neurons, respectively, as detailed in Table 3. The Scaled Exponential Linear Unit function has been used as the activation functions of the hidden layers.

Table 3. Physic-informed neural network architecture

NN branch	Layer	Neurons	Activation function
DefectNet	Input 1	10	SELU
	Dense 1	5	SELU
	Dense 2	1	Linear
MicroNet	Input 2	10	SELU
	Dense 3	5	SELU
	Dense 4	1	Linear
Output	Dense 5	10	ReLU
	Dense 6	5	Linear
	Dense 7	1	Linear
	Custom	-	-

The value of the loss function at each epoch of the training process is reported in Figure 3a, whereas Figure 3b compares the fatigue strength predicted with the NN (S_{NN}) with the experimental values, S_{exp} (an error band of ±150 MPa and a Normal distribution with standard deviation of 50 MPa are also shown).

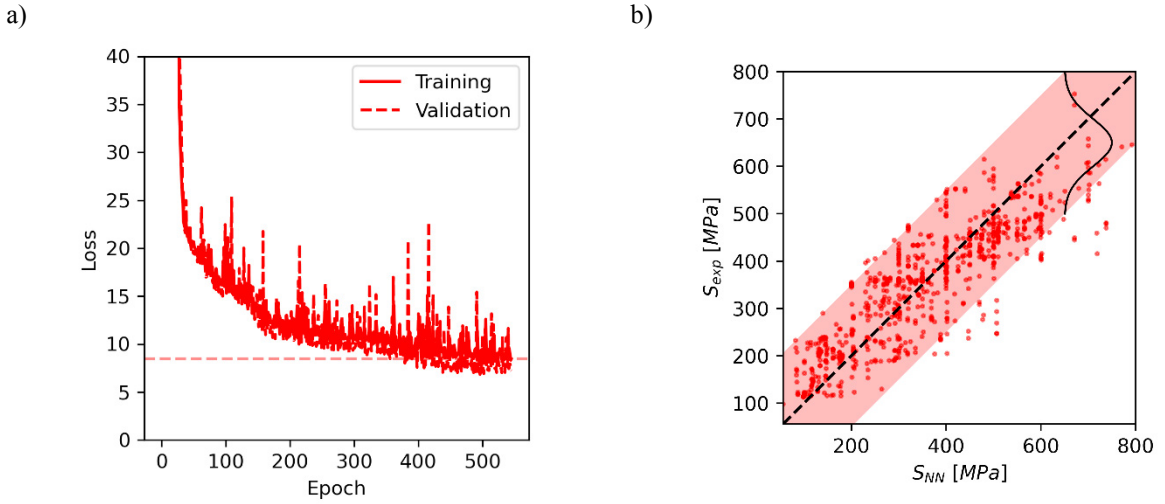

Figure 3. a) Training and validation loss during the training of the NN; b) accuracy plot comparing the prediction of the NN (S_{NN}) with the experimental values (S_{exp}).

According to Figure 3a, the ultimate loss value is below 10, even if the training process is more unstable as it usually occurs for PINN characterized by a complex architecture (or by a loss function), which affects the backpropagation procedure. Figure 3b, the data are concentrated close to the bisector and within the ±150 MPa error band, apart from a limited amount of data.

4.3. NN and PINN: comparison and discussion

The results obtained with the NN and PINN are compared in Figure 4 (datasets in (Du et al., 2021)), where the S-N curve predicted by considering two manufacturing configurations, both included in the training dataset, are reported together with the experimental data.

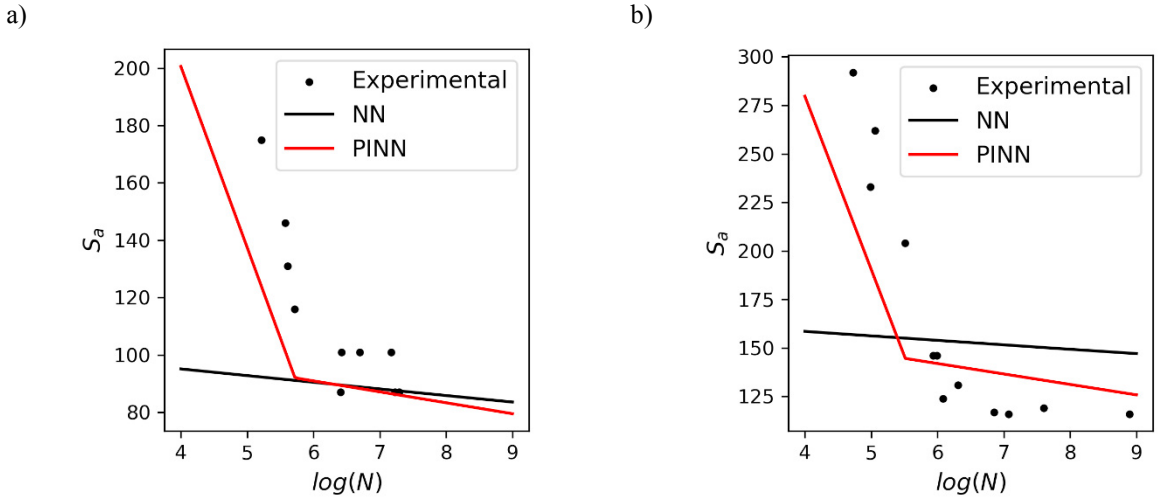

Figure 4. S-N curves predicted with the NN and PINN applied to data from (Du et al., 2021), both contained in the training dataset.

According to Figures 4a and b, the S-N curves predicted with the PINN well fit the experimental data, differently from those predicted with the NN. It is noteworthy that the S-N curves predicted with the PINN are characterized by a bilinear trend typical for metals. On the other hand, the NN hardly replicate the characteristic shape and decreasing trend typical of the S-N curves, because the training process converged preferentially toward a model which predicts a flat curve with a value corresponding to the average of the observed data. This is imputable to the data-hungry characteristic of the traditional ML models that demands a huge amount of data points to effectively learn the relation between the inputs and the outputs of the NN. On the other hand, incorporating the physical knowledge yielded by the Murakami formulation in the PINN leads to a faster convergence of the training process toward a physics-compliant behaviour. Figure 5**Error! Reference source not found.** (Figure 5a for the dataset in (Gong et al., 2015) and Figure 5b for the dataset in (Jiang et al., 2021)) depicts fatigue curves that are predicted with the NN and PINN from manufacturing configurations not present in the training dataset.

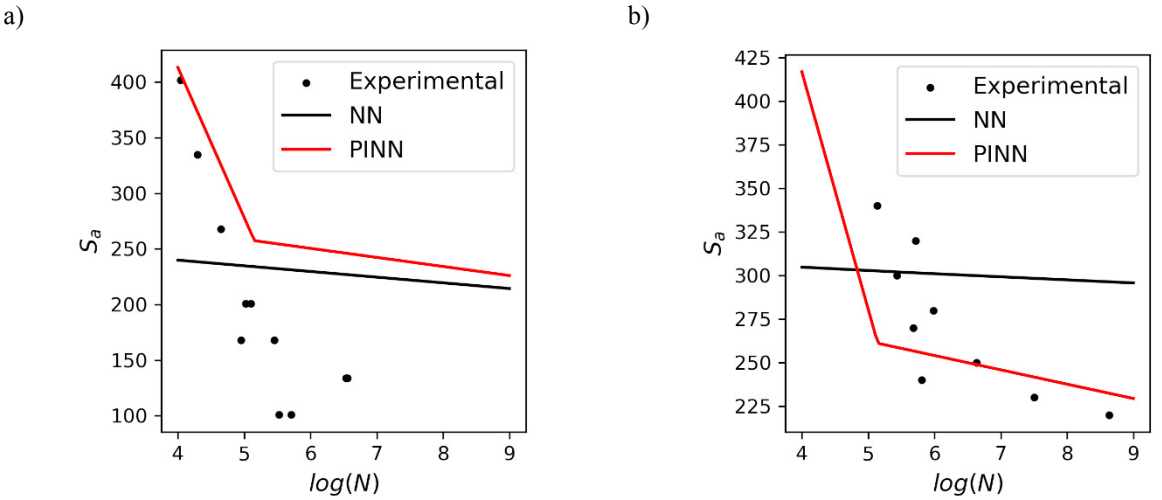

Figure 5. S-N curves predicted with the NN and PINN applied to datasets not considered in the training dataset from: a) (Gong et al., 2015); b) (Jiang et al., 2021).

It can be observed in Figure 6 that the accuracy of the ML methods may decrease when tested outside the training space, overestimating the fatigue strength in the high-cycle fatigue range. However, the decrease in the predictive capability of the PINN is less severe in the validation data from (Jiang et al., 2021), where the predicted behaviour is in good agreement with the experimental data.
To give a complete overview of the model accuracy, the absolute relative errors (ARE) of both the NN and PINN have been reported in the histogram in Figure 6.

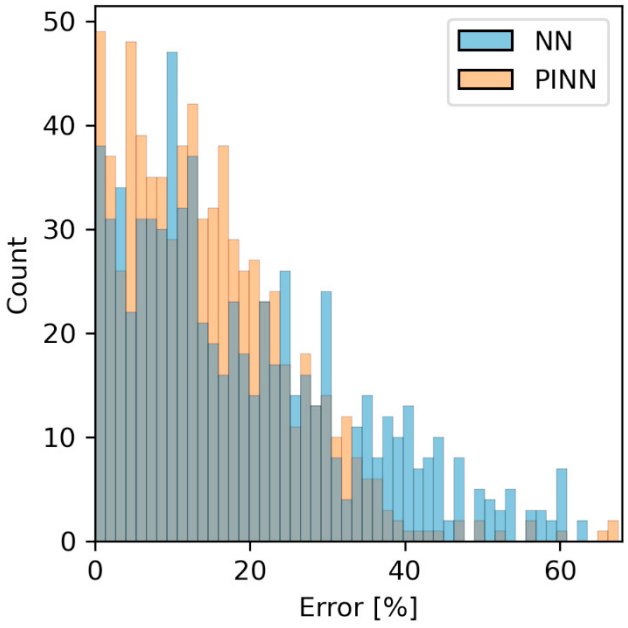

Figure 6. Absolute Relative Error of the NN and PINN prediction compared with the experimental data.

Results reported in Figure 6 show that the PINN has a narrower distribution of the ARE with an average value lower that the one of the NN.

5. Conclusions

In the present work two Machine Learning (ML) algorithms, a Neural Network (NN) algorithm and a Physics-Informed Neural Network (PINN) algorithm, have been developed to predict the stress-life relationship of Ti6Al4V alloys produced through a Selective Laser Melting (SLM) process. The following conclusions can be drawn:

- ML algorithms are capable of modelling the influence of SLM processing parameters, and post-process parameters on the fatigue response of the Ti6Al4V alloy;
- the phenomenological knowledge of the damage-tolerant response of the investigated SLM part can be combined with the NN architecture.
- the combination of the physics-based model with the NN yields more accurate predictions.
- the S-N curve assessed with the PINN model shows physics-compliant trends.

Further investigations will be carried out to model the stochastic nature of the fatigue phenomena with ML algorithms and to explore different ML algorithms and phenomenological hybrid approaches for the assessment of the fatigue properties of parts produced with additive manufacturing.

Acknowledgements

Author sincerely thanks A. Centola for his work on the database curation.

References

Alegre, J. M., Díaz, A., García, R., Peral, L. B., & Cuesta, I. I. (2022). Effect of HIP post-processing at 850 °C/200

MPa in the fatigue behavior of Ti-6Al-4V alloy fabricated by Selective Laser Melting. *International Journal of Fatigue*, *163*(January), 107097. https://doi.org/10.1016/j.ijfatigue.2022.107097

Chen, J., & Liu, Y. (2021). Fatigue property prediction of additively manufactured Ti-6Al-4V using probabilistic physics-guided learning. *Additive Manufacturing*, *39*, 101876. https://doi.org/10.1016/J.ADDMA.2021.101876

Ciampaglia, A., Tridello, A., Paolino, D. S., & Berto, F. (2023). Data driven method for predicting the effect of process parameters on the fatigue response of additive manufactured AlSi10Mg parts. *International Journal of Fatigue*, *170*, 107500. https://doi.org/10.1016/J.IJFATIGUE.2023.107500

Du, L., Qian, G., Zheng, L., & Hong, Y. (2021). Influence of processing parameters of selective laser melting on high-cycle and very-high-cycle fatigue behaviour of Ti-6Al-4V. *Fatigue and Fracture of Engineering Materials and Structures*, *44*(1), 240–256. https://doi.org/10.1111/ffe.13361

du Plessis, A., & Beretta, S. (2020). Killer notches: The effect of as-built surface roughness on fatigue failure in AlSi10Mg produced by laser powder bed fusion. *Additive Manufacturing*, *35*, 101424. https://doi.org/10.1016/J.ADDMA.2020.101424

Eric, W., Claus, E., Shafaqat, S., & Frank, W. (2013). High cycle fatigue (HCF) performance of Ti-6Al-4V alloy processed by selective laser melting. *Advanced Materials Research*, *816–817*(September), 134–139. https://doi.org/10.4028/www.scientific.net/AMR.816-817.134

Fousová, M., Vojtěch, D., Doubrava, K., Daniel, M., & Lin, C. F. (2018). Influence of inherent surface and internal defects on mechanical properties of additively manufactured Ti6Al4V alloy: Comparison between selective laser melting and electron beam melting. *Materials*, *11*(4). https://doi.org/10.3390/ma11040537

Gong, H., Rafi, K., Gu, H., Janaki Ram, G. D., Starr, T., & Stucker, B. (2015). Influence of defects on mechanical properties of Ti-6Al-4V components produced by selective laser melting and electron beam melting. *Materials and Design*, *86*, 545–554. https://doi.org/10.1016/j.matdes.2015.07.147

Günther, J., Krewerth, D., Lippmann, T., Leuders, S., Tröster, T., Weidner, A., Biermann, H., & Niendorf, T. (2017). Fatigue life of additively manufactured Ti–6Al–4V in the very high cycle fatigue regime. *International Journal of Fatigue*, *94*, 236–245. https://doi.org/10.1016/j.ijfatigue.2016.05.018

Günther, J., Leuders, S., Koppa, P., Tröster, T., Henkel, S., Biermann, H., & Niendorf, T. (2018). On the effect of internal channels and surface roughness on the high-cycle fatigue performance of Ti-6Al-4V processed by SLM. *Materials and Design*, *143*, 1–11. https://doi.org/10.1016/j.matdes.2018.01.042

Hu, Y. N., Wu, S. C., Withers, P. J., Zhang, J., Bao, H. Y. X., Fu, Y. N., & Kang, G. Z. (2020). The effect of manufacturing defects on the fatigue life of selective laser melted Ti-6Al-4V structures. *Materials and Design*, *192*. https://doi.org/10.1016/j.matdes.2020.108708

Jiang, Q., Li, S., Zhou, C., Zhang, B., & Zhang, Y. (2021). Effects of laser shock peening on the ultra-high cycle fatigue performance of additively manufactured Ti6Al4V alloy. *Optics and Laser Technology*, *144*(November 2020), 107391. https://doi.org/10.1016/j.optlastec.2021.107391

Kumar, P., & Ramamurty, U. (2020). High cycle fatigue in selective laser melted Ti-6Al-4V. *Acta Materialia*, *194*, 305–320. https://doi.org/10.1016/j.actamat.2020.05.041

Li, J., Yang, Z., Qian, G., & Berto, F. (2022). Machine learning based very-high-cycle fatigue life prediction of Ti-6Al-4V alloy fabricated by selective laser melting. *International Journal of Fatigue*, *158*, 106764. https://doi.org/10.1016/j.ijfatigue.2022.106764

Li, P., Warner, D. H., Fatemi, A., & Phan, N. (2016). Critical assessment of the fatigue performance of additively manufactured Ti-6Al-4V and perspective for future research. *International Journal of Fatigue*, *85*, 130–143. https://doi.org/10.1016/j.ijfatigue.2015.12.003

Macallister, N., & Becker, T. H. (2022). Fatigue life estimation of additively manufactured Ti-6Al-4V: Sensitivity, scatter and defect description in Damage-tolerant models. *Acta Materialia*, *237*, 118189. https://doi.org/10.1016/j.actamat.2022.118189

Maleki, E., Bagherifard, S., Razavi, S. M. J., Bandini, M., du Plessis, A., Berto, F., & Guagliano, M. (2022). On the efficiency of machine learning for fatigue assessment of post-processed additively manufactured AlSi10Mg. *International Journal of Fatigue*, *160*, 106841. https://doi.org/10.1016/j.ijfatigue.2022.106841

Masuo, H., Tanaka, Y., Morokoshi, S., Yagura, H., Uchida, T., Yamamoto, Y., & Murakami, Y. (2018). Influence of defects, surface roughness and HIP on the fatigue strength of Ti-6Al-4V manufactured by additive manufacturing. *International Journal of Fatigue*, *117*, 163–179. https://doi.org/10.1016/J.IJFATIGUE.2018.07.020

Mayer, H., Schuller, R., Fitzka, M., Tran, D., & Pennings, B. (2014). Very high cycle fatigue of nitrided 18Ni maraging steel sheet. *International Journal of Fatigue*, *64*, 140–146. https://doi.org/10.1016/J.IJFATIGUE.2014.02.003

Meneghetti, G., Rigon, D., & Gennari, C. (2019). An analysis of defects influence on axial fatigue strength of maraging steel specimens produced by additive manufacturing. *International Journal of Fatigue*, *118*, 54–64. https://doi.org/10.1016/J.IJFATIGUE.2018.08.034

Mertova, K., Dzugan, J., & Roudnicka, M. (2018). Fatigue properties of SLM-produced Ti6Al4V with various post-processing processes. *IOP Conference Series: Materials Science and Engineering*, *461*(1). https://doi.org/10.1088/1757-899X/461/1/012052

Molaei, R., & Fatemi, A. (2018). Fatigue Design with Additive Manufactured Metals: Issues to Consider and Perspective for Future Research. *Procedia Engineering*, *213*, 5–16. https://doi.org/10.1016/J.PROENG.2018.02.002

Moran, T. P., Carrion, P. E., Lee, S., Shamsaei, N., Phan, N., & Warner, D. H. (2022). Hot Isostatic Pressing for Fatigue Critical Additively Manufactured Ti-6Al-4V. *Materials*, *15*(6), 1–12. https://doi.org/10.3390/ma15062051

Murakami, Y. (2019). Metal fatigue: Effects of small defects and nonmetallic inclusions. *Metal Fatigue: Effects of Small Defects and Nonmetallic Inclusions*, 1–758. https://doi.org/10.1016/C2016-0-05272-5

Murakami, Y., Masuo, H., Tanaka, Y., & Nakatani, M. (2019). Defect Analysis for Additively Manufactured Materials in Fatigue from the Viewpoint of Quality Control and Statistics of Extremes. *Procedia Structural Integrity*, *19*, 113–122. https://doi.org/10.1016/J.PROSTR.2019.12.014

Paolino, D. S., Tridello, A., Chiandussi, G., & Rossetto, M. (2016). *S-N curves in the very-high-cycle fatigue regime: statistical modeling based on the hydrogen embrittlement consideration ORIGINAL CONTRIBUTION*. https://doi.org/10.1111/ffe.12431

Romano, S., Miccoli, S., & Beretta, S. (2019). A new FE post-processor for probabilistic fatigue assessment in the presence of defects and its application to AM parts. *International Journal of Fatigue*, *125*(February), 324–341. https://doi.org/10.1016/j.ijfatigue.2019.04.008

Sanaei, N., & Fatemi, A. (2020). Analysis of the effect of internal defects on fatigue performance of additive manufactured metals. *Materials Science and Engineering A*, *785*(April), 139385. https://doi.org/10.1016/j.msea.2020.139385

Soltani-Tehrani, A., Habibnejad-Korayem, M., Shao, S., Haghshenas, M., & Shamsaei, N. (2022). Ti-6Al-4V powder characteristics in laser powder bed fusion: The effect on tensile and fatigue behavior. *Additive Manufacturing*, *51*(December 2021), 102584. https://doi.org/10.1016/j.addma.2021.102584

Sun, C., Chi, W., Wang, W., & Duan, Y. (2021). Characteristic and mechanism of crack initiation and early growth of an additively manufactured Ti-6Al-4V in very high cycle fatigue regime. *International Journal of Mechanical Sciences*, *205*(March), 106591. https://doi.org/10.1016/j.ijmecsci.2021.106591

Tridello, A., Boursier Niutta, C., Berto, F., Qian, G., & Paolino, D. S. (2021). Fatigue failures from defects in additive manufactured components: A statistical methodology for the analysis of the experimental results. *Fatigue & Fracture of Engineering Materials & Structures*, *44*(7), 1944–1960. https://doi.org/10.1111/FFE.13467

Tridello, A., & Paolino, D. S. (2020). VHCF response of AM materials: A literature review. *Material Design & Processing Communications*, *2*(1), 10–16. https://doi.org/10.1002/mdp2.121

Yadollahi, A., & Shamsaei, N. (2017). Additive manufacturing of fatigue resistant materials: Challenges and opportunities. *International Journal of Fatigue*, *98*, 14–31. https://doi.org/10.1016/J.IJFATIGUE.2017.01.001

Yamashita, Y., Murakami, T., Mihara, R., Okada, M., & Murakami, Y. (2018). Defect analysis and fatigue design basis for Ni-based superalloy 718 manufactured by selective laser melting. *International Journal of Fatigue*, *117*, 485–495. https://doi.org/10.1016/J.IJFATIGUE.2018.08.002

Yan, X., Yin, S., Chen, C., Jenkins, R., Lupoi, R., Bolot, R., Ma, W., Kuang, M., Liao, H., Lu, J., & Liu, M. (2019). Fatigue strength improvement of selective laser melted ti6al4v using ultrasonic surface mechanical attrition. *Materials Research Letters*, *7*(8), 327–333. https://doi.org/10.1080/21663831.2019.1609110

Zhan, Z., & Li, H. (2021a). Machine learning based fatigue life prediction with effects of additive manufacturing process parameters for printed SS 316L. *International Journal of Fatigue*, *142*, 105941. https://doi.org/10.1016/J.IJFATIGUE.2020.105941

Zhan, Z., & Li, H. (2021b). A novel approach based on the elastoplastic fatigue damage and machine learning

models for life prediction of aerospace alloy parts fabricated by additive manufacturing. *International Journal of Fatigue*, *145*, 106089. https://doi.org/10.1016/J.IJFATIGUE.2020.106089

Zhao, X., Li, S., Zhang, M., Liu, Y., Sercombe, T. B., Wang, S., Hao, Y., Yang, R., & Murr, L. E. (2016). Comparison of the microstructures and mechanical properties of Ti-6Al-4V fabricated by selective laser melting and electron beam melting. *Materials and Design*, *95*, 21–31. https://doi.org/10.1016/j.matdes.2015.12.135